

Effective optical response of metamaterials

Guillermo P. Ortiz,¹ Brenda E. Martínez-Zérega,^{2,3} Bernardo S. Mendoza,³ and W. Luis Mochán⁴

¹*Departamento de Física, Facultad de Ciencias Exactas, Universidad Nacional del Nordeste, Avenida Libertad 5400, Campus-UNNE, W3404AAS Corrientes, Argentina*

²*Centro Universitario de los Lagos, Universidad de Guadalajara, Enrique Díaz de León SN, Paseos de la Montaña, Lagos de Moreno, Jalisco 47460, Mexico*

³*Division of Photonics, Centro de Investigaciones en Optica, León, Guanajuato, 37150 Mexico*

⁴*Instituto de Ciencias Físicas, Universidad Nacional Autónoma de México, Apdo. Postal 48-3, 62251 Cuernavaca, Morelos, Mexico*

(Received 22 January 2009; revised manuscript received 8 May 2009; published 26 June 2009)

We use a homogenization procedure for Maxwell's equations in order to obtain in the local limit the frequency-dependent macroscopic dielectric-response tensor $\epsilon_{ij}^M(\omega)$ of metamaterials made of a matrix with inclusions of any geometrical shape repeated periodically with any lattice structure. We illustrate the formalism calculating $\epsilon_{ij}^M(\omega)$ for several structures. For dielectric rectangular inclusions within a conducting material we obtain an anisotropic response that may change from conductorlike at low ω to dielectriclike with resonances at large ω , attaining a very small reflectance at intermediate frequencies which can be tuned through geometrical tailoring. A simple explanation allowed us to predict and confirm similar behavior for other shapes, even isotropic, close to the percolation threshold.

DOI: [10.1103/PhysRevB.79.245132](https://doi.org/10.1103/PhysRevB.79.245132)

PACS number(s): 78.67.Bf, 77.22.Ch, 78.20.Ci, 78.20.Bh

I. INTRODUCTION

Metamaterials are typically binary composites of conventional materials: a matrix with inclusions of a given shape, arranged in a periodic structure. A theoretical model to predict their macroscopic optical properties is very desirable. Since the times of Maxwell, Lord Rayleigh, and Maxwell-Garnet up to today, many authors have contributed to the calculation of the bulk macroscopic response in terms of the dielectric properties of its constituents (for example, see Refs. 1–3) employing various approaches such as variational theories or completely general theories.⁴ The macroscopic effective response can be obtained by defining the microscopic response of a composite, averaging the microscopic fields, and eliminating the contribution of the fluctuating fields to the average of the microscopic response.⁵ Furthermore, the accuracy of the computational method may be confirmed by using general theorems such as Keller's reciprocal theorem.^{6–8}

Recent technologies allow the manufacture of ordered composite materials with periodic structures. For instance, high-resolution electron-beam lithography and its interferometric version have been used in order to make particular designs of nanostructured composites, producing various shapes with nanometric sizes.^{9,10} Moreover, ion-milling techniques are capable of producing high-quality air hole periodic and nonperiodic two-dimensional (2D) arrays, where the holes can have different geometrical shapes.^{11,12} Therefore, it is possible to build devices with different macroscopic optical properties.¹³ For example, a negative refractive index has been predicted and observed¹⁴ for a periodic composite structure of a dielectric matrix with noble-metal inclusions of trapezoidal shape.¹⁵

These advances in metamaterial design have motivated a renewed interest in the study of their optical properties, although the study of the optical properties of composites is not new and several important schemes have been developed

in the past. For example, the macroscopic responses of a bidimensional periodic array of infinite cylinders were calculated in 1959 in terms of the Hertz's potential for a two-dimensional scattering problem.¹⁶ Rayleigh's extended method was applied in order to predict the optical properties of a disordered array of spheres.¹⁷ The variation in the conductivity with the filling fraction of an ordered array of conducting spheres on an insulating matrix has been studied too,¹⁸ and the multipolar effects due to the inhomogeneities of the local field have been analyzed¹⁹ for dielectric spheres at high filling fraction, yielding criteria for their importance as a function of interparticle separation.²⁰ Furthermore, a general theory was developed to describe the electromagnetic response without any reference to a specific representation resulting in a powerful tool to calculate the macroscopic dielectric response.²¹ For periodic composites, a Fourier representation is most fitting and expressions for the bulk macroscopic response may be written in terms of the Fourier coefficients of the microscopic response.^{22–27} On the other hand, a spectral representation theory has allowed the separation of geometric from material properties^{28–30} and it has been employed to study the transport properties of several systems.^{2,3}

In connection with nanostructured metallic films there have been some important developments as well. An exact eigenfunction formulation³¹ and an approximate modal formalism³² were used to explain resonances in the zeroth diffraction order of silver square-wave gratings³¹ and gold-wire gratings.³³ In these works, it was found that resonances might appear due to the excitation of surface modes. Such modes can be excited if their momentum matches that of the incident light after being diffracted by some reciprocal-lattice vector of the periodically structured metal surface. Thus, surface-plasmon-polariton (SPP) modes are excited on the metal-air interface yielding several related phenomena such as an enhancement of optical transmission through sub-wavelength holes.³⁴ Besides the single coupling to SPP modes, double resonant conditions³⁵ and waveguide modes³⁶

seem to play an important role in the enhancement for metallic gratings with very narrow slits and for compound gratings.³⁷

A very strong polarization dependence in the optical response of periodic arrays of oriented subwavelength holes on metal hosts has been recently reported,^{11,12} as well as for a single rectangular inclusion within a perfect conductor.³⁸ The studies above do not rely on SPP excitation as a mechanism to explain the optical results.

In this work we obtain the macroscopic dielectric response of a periodic composite using a homogenization procedure first proposed by Mochán and Barrera⁵ within the context of the local-field effect at crystals, liquids, and disordered composites. In this procedure the macroscopic response of the system is obtained from its microscopic constitutive equations by eliminating the spatial fluctuations of the field with the use of Maxwell's equations and solving for the macroscopic displacement in terms of the macroscopic electric field. Besides the average dielectric function, the formalism above incorporates the effects that the rapidly varying Fourier components of the microscopic response has on the macroscopic response. An equivalent procedure suitable for periodic systems was recently proposed by Halevi and Pérez-Rodríguez³⁹ and applied to photonic crystals and metamaterials. Although developed independently, it may be considered an extension of the generalized local-field-effect theory developed previously by Mochán and Barrera⁵ and it has been applied to the dielectric, magnetic, and in general, the bianisotropic response of photonic crystals. Similar homogenization procedures are also found in Refs. 25–27. We further restrict ourselves to the local limit in which we neglect the dependence of the response on the wavevector, or more precisely, on the Bloch's vector. The macroscopic optical response is obtained in terms of the geometrical shape of the inclusions, their periodic arrangement, and the dielectric function of the host and the inclusions. The proposed scheme is straightforward requiring standard numerical computations. It has the advantage of fully accounting for the detailed geometry of the system. For systems with periods much smaller than the wavelength of the incoming light, the local limit becomes the exact response while it accounts for the local-field effect, i.e., the interaction among parts of the system through the spatially fluctuating electromagnetic field. We reproduce previously reported results^{23,30,40} and effects resulting solely from the geometrical shape of the inclusions, namely, the existence of transparency windows within metal-dielectric metamaterials slightly above the percolation threshold of the metallic phase.

The paper is organized as follows. In Sec. II we present the theoretical approach used for the calculation of the macroscopic dielectric response of the composite. In Sec. III we validate our formalism comparing it with previous schemes, yielding very good agreement. Then, we present results for a two-dimensional periodic structure consisting of a gold host with dielectric rectangular prism or circular inclusions. Finally, in Sec. IV we present our conclusions.

II. THEORETICAL APPROACH

In order to calculate the macroscopic dielectric response of a metamaterial we follow the steps of Ref. 5. We start by

defining appropriate average and fluctuation idempotent projectors \hat{P}_a and $\hat{P}_f = \hat{1} - \hat{P}_a$ such that \hat{P}_a acting on any microscopic field \mathbf{F} produces its macroscopic projection $\mathbf{F}^M \equiv \hat{P}_a \mathbf{F} \equiv \hat{P}_a \mathbf{F}$ while \hat{P}_f acting on the same field yields the spatially fluctuating part $\mathbf{F}_f \equiv \hat{P}_f \mathbf{F} = \mathbf{F} - \mathbf{F}^M$, which we wish to eliminate. The constitutive equation $\mathbf{D} = \hat{\epsilon} \mathbf{E}$, where $\hat{\epsilon}$ is the dielectric operator (in the general case, a complex tensorial integral operator for each frequency), may be split into macroscopic and spatially fluctuating parts. Thus we write

$$\mathbf{D}^M = \hat{\epsilon}_{aa} \mathbf{E}^M + \hat{\epsilon}_{af} \mathbf{E}_f, \quad (1)$$

where $\hat{O}_{\alpha\beta} = \hat{P}_\alpha \hat{O} \hat{P}_\beta$ ($\alpha, \beta = a, f$) for any operator \hat{O} and we used the idempotency of the projectors. Furthermore, the fluctuating part of the wave equation for a nonmagnetic material is given by

$$\nabla \times (\nabla \times \mathbf{E}_f) = k_0^2 \mathbf{D}_f = k_0^2 (\hat{\epsilon}_{fa} \mathbf{E}^M + \hat{\epsilon}_{ff} \mathbf{E}_f), \quad (2)$$

where $k_0 = \omega/c = 2\pi/\lambda_0$ and λ_0 are the free-space wave number and wavelength corresponding to frequency ω and we assumed that the external sources have no spatial fluctuations (otherwise, a homogenization procedure would prove useless). We solve Eq. (2) for the fluctuating electric field

$$\mathbf{E}_f = - \left(\hat{\epsilon}_{ff} - \frac{1}{k_0^2} (\nabla \times \nabla \times)_{ff} \right)^{-1} \hat{\epsilon}_{fa} \mathbf{E}^M, \quad (3)$$

where $\nabla \times \nabla \times$ denotes the operator (grad div - ∇^2) and the inverse on the right-hand side (RHS) may be interpreted in real space as a Green's function, i.e., an integral operator whose kernel obeys a differential equation with a singular source. The inverse in the second term in the RHS of Eq. (3) is performed *after* the projections onto the space of fluctuating fields, denoted by the two subscripts *ff*. Finally, we substitute Eq. (3) into Eq. (1) to obtain the macroscopic relation $\mathbf{D}^M = \hat{\epsilon}^M \mathbf{E}^M$, where we identify the macroscopic dielectric operator

$$\hat{\epsilon}^M = \hat{\epsilon}_{aa} - \hat{\epsilon}_{af} \left[\hat{\epsilon}_{ff} - \frac{1}{k_0^2} (\nabla \times \nabla \times)_{ff} \right]^{-1} \hat{\epsilon}_{fa}. \quad (4)$$

The first term in the RHS of Eq. (4) represents the average dielectric response while the second term incorporates the effect of the interactions through the small-length-scale spatial fluctuations of the field on the macroscopic response.

We rewrite Eq. (4), which corresponds to Eq. (21) of Ref. 5, as

$$\hat{\epsilon}^M = \hat{\epsilon}_{aa} - \hat{\epsilon}_{af} \hat{\Phi}_{fa}, \quad (5)$$

where $\hat{\Phi}_{fa}$ is defined through

$$\hat{\mathcal{W}}_{ff} \hat{\Phi}_{fa} = \hat{\epsilon}_{fa} \quad (6)$$

and we introduced the wave operator

$$\hat{\mathcal{W}} = \hat{\epsilon} - \frac{1}{k_0^2} \nabla \times \nabla \times. \quad (7)$$

For a periodic system, we can use Bloch's theorem to represent the fields and operators through their Fourier components

$$\mathbf{F}_{\mathbf{q}}(\mathbf{r}) = \sum_{\mathbf{G}} \mathbf{F}_{\mathbf{q}}(\mathbf{G}) e^{i(\mathbf{q}+\mathbf{G})\cdot\mathbf{r}}, \quad (8)$$

$$\mathcal{O}_{\mathbf{q}}(\mathbf{r}, \mathbf{r}') = \sum_{\mathbf{G}, \mathbf{G}'} \mathcal{O}_{\mathbf{q}}(\mathbf{G}, \mathbf{G}') e^{i[(\mathbf{q}+\mathbf{G})\cdot\mathbf{r} - (\mathbf{q}+\mathbf{G}')\cdot\mathbf{r}']}, \quad (9)$$

where $\mathbf{F}_{\mathbf{q}}(\mathbf{r})$ denotes an arbitrary position-dependent field with a given Bloch vector \mathbf{q} , $\mathcal{O}_{\mathbf{q}}(\mathbf{r}, \mathbf{r}')$ is the kernel corresponding to an arbitrary operator $\hat{\mathcal{O}}$ for the same Bloch vector, and \mathbf{G} and \mathbf{G}' are reciprocal vectors. In this case we can chose \hat{P}_a as a truncation operator in reciprocal space that eliminates the Fourier components outside of the first Brillouin zone, which can be represented by a Kronecker's delta $\hat{P}_a \rightarrow \delta_{\mathbf{G}0}$. Also, we can identify ∇ with a diagonal block matrix $i(\mathbf{q}+\mathbf{G})\delta_{\mathbf{G},\mathbf{G}'}$. Thus, we rewrite Eqs. (5)–(7) as

$$[\epsilon_{\mathbf{q}}^M]_{ik} = [\epsilon_{\mathbf{q}}(\mathbf{0}, \mathbf{0})]_{ik} - \sum_j \sum_{\mathbf{G} \neq 0} [\epsilon_{\mathbf{q}}(\mathbf{0}, \mathbf{G})]_{ij} [\Phi_{\mathbf{q}}(\mathbf{G}, \mathbf{0})]_{jk}, \quad (10)$$

$$\sum_j \sum_{\mathbf{G}' \neq 0} [\mathcal{W}_{\mathbf{q}}(\mathbf{G}, \mathbf{G}')]_{ij} [\Phi_{\mathbf{q}}(\mathbf{G}', \mathbf{0})]_{jk} = [\epsilon_{\mathbf{q}}(\mathbf{G}, \mathbf{0})]_{ik}, \quad (11)$$

and

$$[\mathcal{W}_{\mathbf{q}}(\mathbf{G}, \mathbf{G}')]_{ij} = [\epsilon_{\mathbf{q}}(\mathbf{G}, \mathbf{G}')]_{ij} + \frac{1}{k_0^2} \delta_{\mathbf{G},\mathbf{G}'} \sum_{kl} \delta_{ij}^{kl} (q_k + G_k)(q_l + G_l). \quad (12)$$

As the fields are vector valued for each reciprocal vector, our operators are matrix valued for each pair of reciprocal vectors. Thus, in the equations above we introduced explicitly the Cartesian indices $ijkl$. We also introduced the usual four-index delta function $\delta_{ij}^{kl} = \delta_{ik}\delta_{lj} - \delta_{il}\delta_{jk}$. Notice that \mathbf{G} and \mathbf{G}' are different from zero in Eqs. (10)–(12), as they involve the fluctuating fields. Our Eqs. (10)–(12) are closely related to Eq. (35) of Ref. 39. We remark that in the long-wavelength limit $G/k_0 \gg 1$ so that the transverse part of the RHS of Eq. (12) is dominated by its large second term. Thus, from Eq. (11), the transverse part of $\Phi_{\mathbf{q}}(\mathbf{G}, \mathbf{0})$ becomes small, on the order of k_0^2/G^2 . Nevertheless, the second term on the RHS of Eq. (12) does not affect the longitudinal part of $\mathcal{W}_{\mathbf{q}}(\mathbf{G}, \mathbf{G}')$ so that the longitudinal part of $\Phi_{\mathbf{q}}(\mathbf{G}, \mathbf{0})$ becomes dominant in this limit. This means that in the long-wavelength limit, the fluctuations are mostly longitudinal⁵ and we may neglect retardation in their calculation.

We consider now a two-component system made up of a homogeneous host with a local isotropic dielectric function ϵ_h , in which arbitrarily shaped particles with a local isotropic dielectric function ϵ_p are periodically included. Then,

$$[\epsilon_{\mathbf{q}}(\mathbf{G}, \mathbf{G}')]_{ij} = [\epsilon_h \delta_{\mathbf{G},\mathbf{G}'} + \epsilon_{ph} S(\mathbf{G} - \mathbf{G}')] \delta_{ij}, \quad (13)$$

where $\epsilon_{ph} \equiv \epsilon_p - \epsilon_h$. The Fourier coefficients,

$$S(\mathbf{G}) = \frac{1}{\Omega} \int S(\mathbf{r}) e^{i\mathbf{r}\cdot\mathbf{G}} d\mathbf{r} = \frac{1}{\Omega} \int_v e^{i\mathbf{r}\cdot\mathbf{G}} d\mathbf{r}, \quad (14)$$

characterize completely the shape of the particle, as the integrals are over the volume v occupied by the inclusions

within a single unit cell whose total volume is Ω . Here, we introduced the characteristic function $S(\mathbf{r})$ whose value is $S(\mathbf{r})=1$ within v and $S(\mathbf{r})=0$ outside v . In particular,

$$S(\mathbf{G} = \mathbf{0}) = v/\Omega \equiv f, \quad (15)$$

with f as the filling fraction of the inclusions and

$$[\epsilon_{\mathbf{q}}(\mathbf{0}, \mathbf{0})]_{ij} = (\epsilon_h + \epsilon_{ph}f) \delta_{ij}. \quad (16)$$

Notice that for local response $[\epsilon_{\mathbf{q}}(\mathbf{G}, \mathbf{G}')]_{ij}$ depends only on the difference $\mathbf{G} - \mathbf{G}'$ and it does not depend on \mathbf{q} .

Finally, substituting Eq. (13) in Eq. (10) and taking the local $\mathbf{q} \rightarrow \mathbf{0}$ limit, we obtain

$$\epsilon_{ij}^M \equiv [\epsilon_{\mathbf{0}}^M]_{ij} = (\epsilon_h + \epsilon_{ph}f) \delta_{ij} - \epsilon_{ph} \sum_{\mathbf{G} \neq 0} S(-\mathbf{G}) [\Phi_{\mathbf{0}}(\mathbf{G}, \mathbf{0})]_{ij}, \quad (17)$$

where $[\Phi_{\mathbf{0}}(\mathbf{G}, \mathbf{0})]_{ij}$ is obtained by solving Eq. (11) after substituting Eq. (13) and

$$[\mathcal{W}_{\mathbf{0}}(\mathbf{G}, \mathbf{G}')]_{ij} = [\epsilon_h \delta_{\mathbf{G},\mathbf{G}'} + \epsilon_{ph} S(\mathbf{G} - \mathbf{G}')] \delta_{ij} - \frac{1}{k_0^2} (G^2 \delta_{ij} - G_i G_j) \delta_{\mathbf{G},\mathbf{G}'}, \quad (18)$$

from Eq. (12). Notice that in principle we could take the local limit $\mathbf{q} \rightarrow \mathbf{0}$ without also taking the long-wavelength limit $k_0 \rightarrow 0$, although it is advisable to verify that $\epsilon_{\mathbf{q}}^M$ is close to $\epsilon_{\mathbf{0}}^M = \epsilon^M$ for the relevant wave vectors \mathbf{q} that appear in each particular application. We remark that the first term on the RHS of Eq. (17) is isotropic as it is simply the average of the response of the constituents, which we took to be local, piecewise homogeneous, and isotropic. Nevertheless, the second term includes information on the geometry of the system including both the shapes of the particles and their periodic arrangement. Thus, in general it yields a nonisotropic contribution to the macroscopic dielectric tensor. In the following section we show several examples of this procedure to calculate the macroscopic dielectric tensor ϵ_{ij}^M .

III. RESULTS

A. Comparison to previous work

In this section we apply our results to light moving across a 2D square array of infinite square dielectric prisms with diagonals aligned with the sides of the square primitive cell, a system previously proposed by Milton *et al.*⁴⁰ We chose the parameters $\epsilon_p=5.0$, $\epsilon_h=1.0$, and $f=0.3$. We take a finite free-space wavelength $\lambda_0=10L$, with L as the lattice parameter, so that, according to Eq. (18) we expect only small retardation effects on the order of $(L/\lambda_0)^2=1/100$. We choose the polarization normal to the prisms axis so that in our local limit the system is effectively isotropic in 2D. We truncated our matrices in reciprocal space by setting a maximum value $2\pi n_{\max}/L$ for the magnitude $|G_x|$ and $|G_y|$ of the components of the reciprocal vectors so for a field polarization within the plane the number of rows and columns for the matrix $[\mathcal{W}_{\mathbf{0}}(\mathbf{G}, \mathbf{G}')]_{ij}$ in Eq. (18) is given by $8n_{\max}(n_{\max}+1)$. To test the convergence of our computational procedure, in Fig. 1 we show our results for $\epsilon_{ij}^M \equiv \epsilon^M \delta_{ij}$ as a function of the maxi-

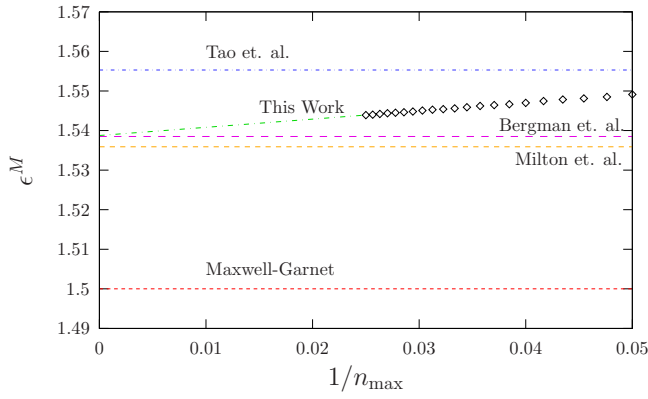


FIG. 1. (Color online) We show the normal-to-the-axis macroscopic dielectric function ϵ^M obtained through Eq. (17) for a 2D square array with lattice parameter L of square dielectric prisms with response $\epsilon_p=5.0$ placed in vacuum with filling fraction $f=0.3$ for a free-space wavelength $\lambda_0=10L$ as a function of the largest reciprocal-vector index vs $1/n_{\max}$. We show a linear extrapolation of our results toward $1/n_{\max} \rightarrow 0$ and we indicate the values predicted by Maxwell-Garnet formula and by some other authors mentioned in the text.

imum index n_{\max} . From Fig. 1 we see that ϵ^M converges approximately as $1/n_{\max}$ and values of the order around $n_{\max}=40$ are needed to obtain an accuracy better than 0.5% without extrapolating, yielding large matrices of more than $13\,000 \times 13\,000$ elements. In the same figure we have indicated the response obtained by Milton *et al.*,²⁹ Tao *et al.*,²³ and Bergman *et al.*,³⁰ which studied the same composite. As we see, linear extrapolation of our results toward $1/n_{\max} \rightarrow 0$ converge to those Bergman *et al.* and of Milton *et al.* whereas the result of Tao *et al.* differs slightly. Finally, we also compare our results with those of mean-field theory, as embodied in Maxwell-Garnet’s (MG) formulae

$$\epsilon^M = \epsilon_h + f\epsilon_{ph} - \frac{\epsilon_{ph}^2 f(1-f)}{\gamma\epsilon_h + \epsilon_{ph}(1-f)}, \quad (19)$$

with $\gamma=2$ for our 2D system.²⁷ As we see in the figure, the MG results differ from ours and the other authors’ results mainly due to its intrinsic limitations.²⁷ We have checked our results with other set of parameters also reported by the same cited authors and we have obtained similar agreement as mentioned above. The rate of convergence of our method is similar to that reported in Ref. 41 when written in terms of n_{\max} .

We can also test the convergence of our results above using Keller’s theorem,^{6–8} which we may write as $K=K_x K_y=1$, where we define Keller’s coefficients along principal axes x, y as $K_x=(\epsilon_x^M \tilde{\epsilon}_x^M)/(\epsilon_h \epsilon_p)$ and $K_y=(\epsilon_y^M \tilde{\epsilon}_y^M)/(\epsilon_h \epsilon_p)$. Here, we introduced the macroscopic response $\tilde{\epsilon}_x^M$ and $\tilde{\epsilon}_y^M$ of the reciprocal system that is obtained from the original system by interchanging $\epsilon_h \leftrightarrow \epsilon_p$. Indeed, for our isotropic system we expect $K_x=1$ as $K_x=K_y$. In Fig. 2 we show K_x-1 vs $1/n_{\max}$ for the system corresponding to Fig. 1. We see clearly that K_x-1 decreases linearly in $1/n_{\max}$. However, its extrapolation toward $n_{\max} \rightarrow \infty$ does not attain the value $K_x-1=0$ as expected from Keller’s theorem. The reason for the small

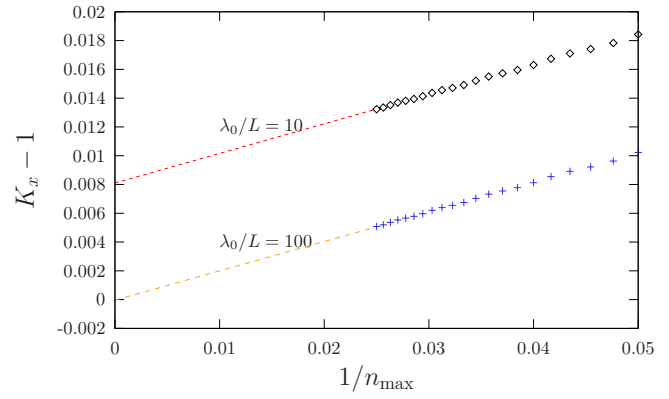


FIG. 2. (Color online) Keller’s coefficient K_x-1 as a function of $1/n_{\max}$ and its linear extrapolation toward $n_{\max} \rightarrow \infty$ for the same system as in Fig. 1 in the cases of $\lambda_0/L=10$ and 100.

discrepancy is that our calculation includes retardation effects which we expect to be of order $(L/\lambda_0)^2$ while Keller’s theorem is strictly valid only in systems with no retardation. To confirm this statement, we also display in Fig. 2 the results of a calculation for $\lambda_0=100L$, showing that in this case, the discrepancy between the extrapolated and the expected value is negligible. Thus, we have verified that our calculation is consistent with Keller’s theorem in the absence of retardation and has an error that goes to zero as $1/n_{\max}$ when $\lambda_0/L \rightarrow \infty$.

In Fig. 3 we show nearly converged (error $<0.5\%$) results for ϵ^M as a function of the filling fraction f for the same system as in Fig. 1. We can see again an excellent agreement of our results with those obtained by Milton *et al.*, and Bergman *et al.*, and, to a lesser extent, with those of Tao *et al.* The MG results are noticeably lower with a discrepancy that increases with filling fraction. We have obtained results identical to ours in Figs. 1 and 3 using Eq. (35) of Ref. 39, confirming that our formalism is equivalent to that of Halevi and Pérez-Rodríguez. In conclusion, our approach does indeed reproduce the results of other works and thus we have validated our numerical scheme and can be confident on the accuracy of our results.

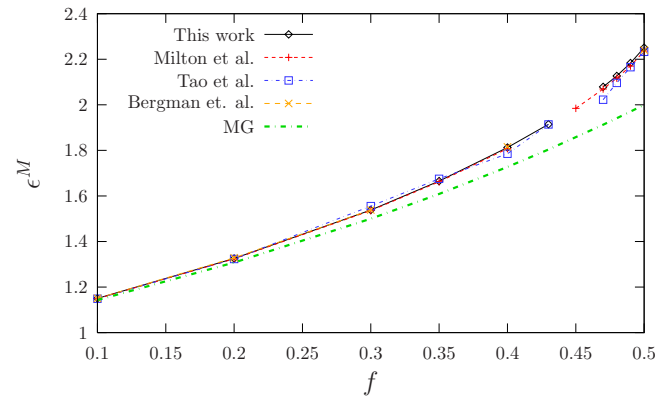


FIG. 3. (Color online) ϵ^M versus the filling fraction for the same system as shown in Fig. 1. Our result was obtained from Eqs. (17) and (18) employing a $13\,120 \times 13\,120$ matrix $[\mathcal{W}_0(\mathbf{G}, \mathbf{G}')]_{ij}$.

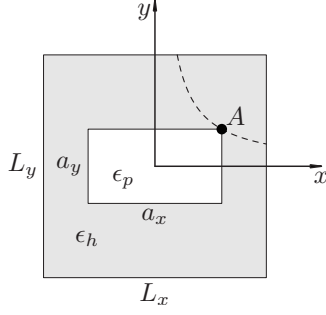


FIG. 4. Unit cell of a 2D rectangular array of rectangular prisms with response ϵ_p within a host with response ϵ_h . The aspect ratio of the rectangles is determined by the point $A=(L_x\xi_x, L_yf/\xi_x)$ that lies on the dashed line from (L_xf, L_y) to (L_x, L_yf) .

B. 2D array

Having confirmed our calculation procedure through comparison to earlier works and convergence tests, we proceed to evaluate the optical properties of a metamaterial. We choose a 2D rectangular lattice of rectangular prisms assuming translational symmetry along z (see Fig. 4). The unit cell has lengths L_x and L_y along the x and y directions and the inclusions have corresponding sizes a_x and a_y . The shape of the lattice is controlled by a parameter η defined through

$$L_x = \eta L_y, \quad (20)$$

and we define

$$\xi_i \equiv \frac{a_i}{L_i}, \quad i = x, y. \quad (21)$$

Then,

$$\mathbf{G} = n_x \frac{2\pi}{L_x} \hat{x} + n_y \frac{2\pi}{L_y} \hat{y} = \frac{2\pi}{L_x} (n_x \hat{x} + \eta n_y \hat{y}), \quad (22)$$

for integer n_x and n_y , and

$$f = \xi_x \xi_y. \quad (23)$$

From Eq. (14) we obtain

$$\begin{aligned} S(\mathbf{G}) &= \sin c\left(\frac{G_x a_x}{2}\right) \sin c\left(\frac{G_y a_y}{2}\right) \\ &= \sin c(\pi \xi_x n_x) \sin c\left(\pi \frac{f}{\xi_x} n_y\right), \end{aligned} \quad (24)$$

where $\sin c(x) = \sin(x)/x$. We can vary the shape of the inclusion keeping the filling fraction fixed by simply changing ξ_x within the bounds

$$f \leq \xi_x \leq 1. \quad (25)$$

The array is square if $L_x = L_y$. Furthermore, if $\xi_x = \xi_y = \sqrt{f}$ the inclusions have a square cross section while for $\xi_x > \sqrt{f}$ ($\xi_x < \sqrt{f}$) they become elongated along x (y). For $\xi_x = 1$ and $\xi_y = f$ ($\xi_x = f$ and $\xi_y = 1$) the inclusions fully occupy the unit cell along x (y), contacting neighbor inclusions, so that the system becomes an effectively one-dimensional system of slabs with surfaces normal to y (x).

To interpret the results easily we consider a semi-infinite slab $z > 0$ cut out of our metamaterial and we calculate its normal-incidence reflectance

$$R_\zeta = \left| \frac{\sqrt{\epsilon_{\zeta\zeta}^M} - 1}{\sqrt{\epsilon_{\zeta\zeta}^M} + 1} \right|^2, \quad (\zeta = x, y) \quad (26)$$

corresponding to a $\zeta = x, y$ linearly polarized incoming beam propagating through empty space along z and impinging upon the interface which we locate at $z=0$. In this equation we have neglected the possibility of a magnetic permeability $\mu \neq 1$, which may be expected even when the constituents of the system are nonmagnetic due to the possible nonlocality of the macroscopic dielectric response ϵ_q^M , as may be obtained from Eq. (10). The nonlocality may be partially accounted for by a local dielectric function $\epsilon^M = \epsilon_0^M$ and a local magnetic permeability μ , which is on the order of $\mu - 1 \sim (\epsilon_q^M - \epsilon_0^M)/q^2$.³⁹ From Eq. (12), we expect $\mu - 1 \sim k_0^2 L^2$, where L is on the order of the periodicity of the system. Another criteria that has been developed for conducting structures states that the magnetic response may be neglected as long as the cross section of the particles is much smaller than the penetration depth.⁴² Thus, in the examples that follow we may safely neglect the magnetic permeability.

In the following figures we choose a square unit cell with $L_x = L_y = 40$ nm with gold in the interstitial region, for which we use the experimentally determined response $\epsilon_h = \epsilon(\text{Au})$,⁴³ and with dielectric inclusions for which we chose $\epsilon_p = 4$. For different values for the filling fraction f we control the rectangular geometry of the inclusion with the parameter ξ_x . The value of n_{\max} is set to 50, which gives good converged results.⁴⁴

We start with the extreme case $\xi_x = 1$, for which we have a system of alternating conductor and dielectric flat slabs piled up along the y direction. In this case, the nonretarded macroscopic dielectric response is given exactly by

$$\epsilon_{xx}^M = f\epsilon_p + (1-f)\epsilon_h \quad (27)$$

and

$$\frac{1}{\epsilon_{yy}^M} = \frac{f}{\epsilon_p} + \frac{1-f}{\epsilon_h}. \quad (28)$$

The latter expression can be written as

$$\epsilon_{yy}^M = \epsilon_h + f\epsilon_{ph} - \frac{\epsilon_{ph}^2 f(1-f)}{\epsilon_h + \epsilon_{ph}(1-f)}, \quad (29)$$

which is the MG result for one dimension, i.e., Eq. (19) with $\gamma=1$.

In Fig. 5 we show R_ζ vs the photon energy $\hbar\omega$ as obtained through our numerical scheme [Eq. (17)] and compare them with the exact nonretarded results [Eqs. (27) and (29)]. We remark that both numerical and exact results agree closely. Actually, in the Appendix we show analytically that in this case our formalism coincides exactly with Eqs. (27)–(29) and that Eq. (27) holds also along the translational invariant direction of 2D systems.²⁵

The system is highly anisotropic ($R_x \neq R_y$) so that the one-dimensional (1D) MG results are only applicable along the y

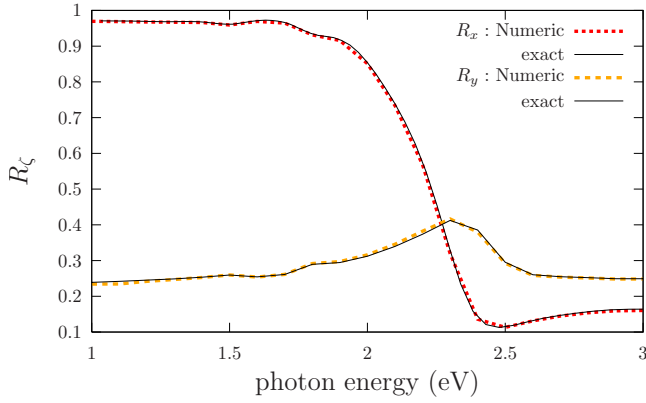


FIG. 5. (Color online) Reflectance R_ζ ($\zeta=x,y$) vs photon energy for $\xi_x=1$, i.e., for a 1D multilayer of alternating slabs of gold [$\epsilon_h = \epsilon(\text{Au})$] and a dielectric ($\epsilon_p=4$), with $L=40$ nm and $f=0.5$. The slabs are normal to the y direction and the incoming light propagates along the z direction. We compare numerical results obtained from Eq. (17) with the exact nonretarded results obtained through Eq. (27) for R_x and Eq. (28) or Eq. (29) (Maxwell-Garnet in 1D) for R_y .

direction (R_y). Notice that the behavior of the system at low frequencies is metallic for $\zeta=x$, with a very high reflectance, while it is dielectriclike for $\zeta=y$, as electric the current may flow unimpeded through the Au layers in the x direction but it would be interrupted along the y direction by the dielectric layers.

Having checked that our approach coincides with two well-known analytic limits, we proceed to show results for other choices of ξ_x and f . In Fig. 6 we show the reflectance R_ζ for inclusion with three rectangular cross sections with a fixed $\xi_y=0.5$ for several choices of $\xi_x=0.5, 0.7$, and 0.9 , with corresponding values of $f=0.25, 0.35$, and 0.45 . Thus, we include square and rectangular prisms. As could be expected, $R_x=R_y$ for the square isotropic case $\xi_x=\xi_y$ while for rectangular sections the reflectance becomes strongly dependent on the polarization $\zeta=x$ or y ; the anisotropy increases as ξ_x moves away from ξ_y . As ϵ_p and ϵ_h are isotropic, the anisotropy $\epsilon_x^M \neq \epsilon_y^M$ of the macroscopic response arises from the

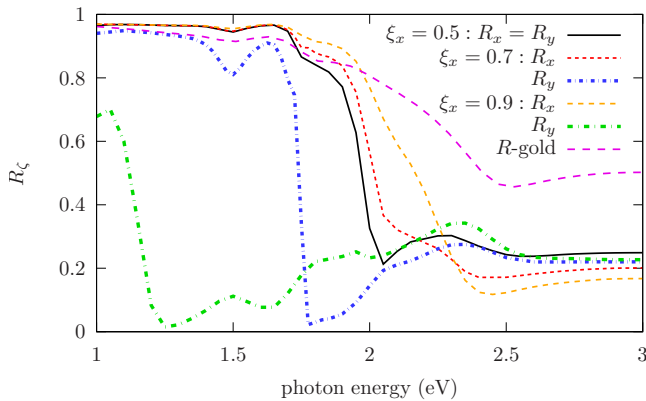


FIG. 6. (Color online) Reflectance R_x (thin lines) and R_y (thick lines) vs the photon energy, for a gold host with inclusions of $\epsilon_p = 4$ and a fixed $\xi_y=0.5$, for three different values of $\xi_x=0.5, 0.7$, and 0.9 (see text for details). We also show the reflectivity of gold.

last term of Eq. (17). Thus, the source of the anisotropy is the local-field interaction among the inclusions, linked to the geometry of the system.

We notice that R_ζ for $\zeta=x$ polarization, along the elongated side of the rectangles, is qualitatively similar to the isotropic case, as well as to that of gold (shown in the same Fig. 6). To wit, for low energies the reflectance is very large, as gold behaves like a Drude metal and most of the light is reflected. For higher energies and especially above the interband-transitions threshold of gold (~ 2.44 eV), the reflectance diminishes as gold deviates from the pure Drude-type behavior and dissipation mechanisms beyond Ohmic heating appear. It is important to note that the surface and bulk plasma frequencies ($\sim 5, 6$ eV) are still higher up in energy than such threshold.

However, we notice an interesting effect for $\zeta=y$ polarization along the short side of the rectangles. At some energies R_y deviates strongly from the isotropic case as ξ_x increases, and shows a counterintuitive behavior, developing a deep minimum that approaches zero reflectance for some values of the photon energy. This may appear surprising, as gold is very reflective in the infrared region. Nevertheless the geometry of the inclusions changes this behavior dramatically. It is also interesting to note that above the interband threshold the anisotropy is drastically reduced as $R_x \sim R_y$.

To explain the surprising behavior of the reflectance, in Fig. 7 we show the real and imaginary parts of the macroscopic response ϵ_{yy}^M for the same system as the one presented in Fig. 6. For $\xi_x > \xi_y$ the response along y is dielectriclike, with a positive $\text{Re}(\epsilon_{yy}^M)$ larger than unity, not unlike the 1D layered system presented in Fig. 5. Nevertheless, as the dielectric prisms are completely isolated from each other by the metallic interstices, the Au region percolates and the behavior at low enough frequencies is metallic, with a negative ϵ_{yy}^M . Thus, there is a photon energy where $\text{Re}(\epsilon_{yy}^M)$ crosses through unity. This energy is redshifted as ξ_x grows and the metallic behavior disappears completely at the limit $\xi_x=1$. Thus, for appropriate values of ξ_x , the crossing may be situated at frequencies too low to excite interband transitions in Au but large enough so that Ohmic losses become unimportant. For that frequency at which $\text{Re}(\epsilon_{yy}) \approx 1$ and $\text{Im}(\epsilon_{yy}) \ll 1$ there is a good impedance matching between vacuum and the material and thus, there is a small reflectance that approaches zero. When this conditions holds, the transmittance of a finite slab approaches unity. Our results show that this is the case at $\hbar\omega \approx 1.25(1.7)$ eV for $\xi_x=0.9$ ($\xi_x=0.7$).

We explained the different behaviors between the x and y response of a system of rectangular prisms for different values of ξ_x and different frequencies in terms of a low-frequency metallic and high-frequency insulating behavior of the composite, which in turn is related to the percolation of the metallic host. We may confirm these ideas by studying other systems with dielectric inclusions within a percolating conducting host such as a square array of dielectric cylinders within an Au host. For a filling fraction $f > \pi/4$ the dielectric cylinders would touch each other impeding the flow of current between the conducting regions that would become isolated from each other and the system would behave as an insulator. Thus, we study the case $f < \pi/4$ for which we expect the low-frequency behavior to be metalliclike with a

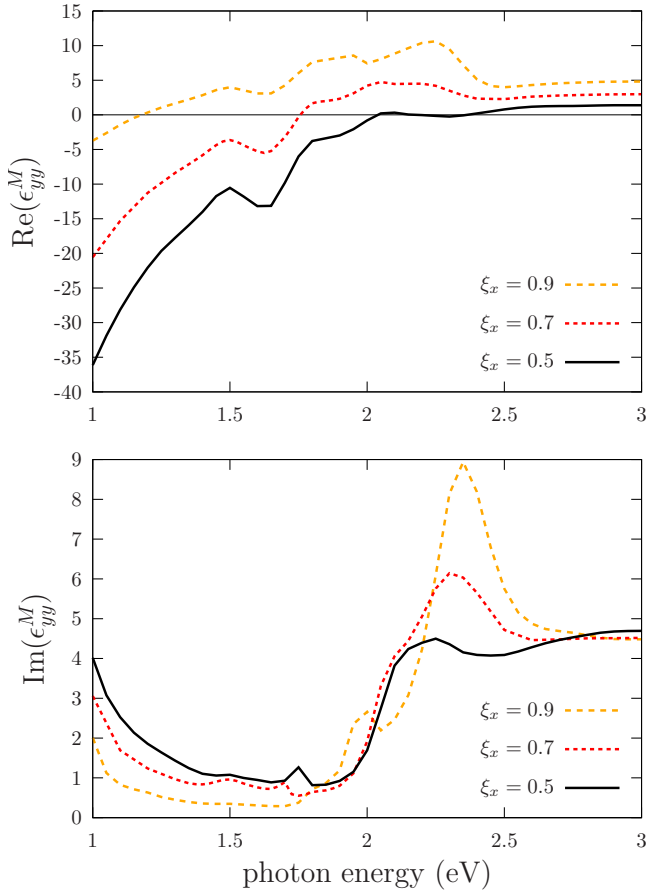


FIG. 7. (Color online) Real (top panel) and imaginary (bottom panel) parts of ϵ_{yy}^M vs photon energy for the same system as that presented in Fig. 6.

transition into a dielectriclike behavior at higher frequencies as in the rectangular case. This system is however isotropic, $R_x=R_y=R$. To perform the calculation we only require the Fourier coefficients $S(\mathbf{G})=2fJ_1(Gr_c)/Gr_c$, with r_c as the radius of the inclusions and J_1 as the J -Bessel function of order 1. Figure 8 shows that R indeed attains large values at low frequencies, corresponding to a metallic behavior, and then

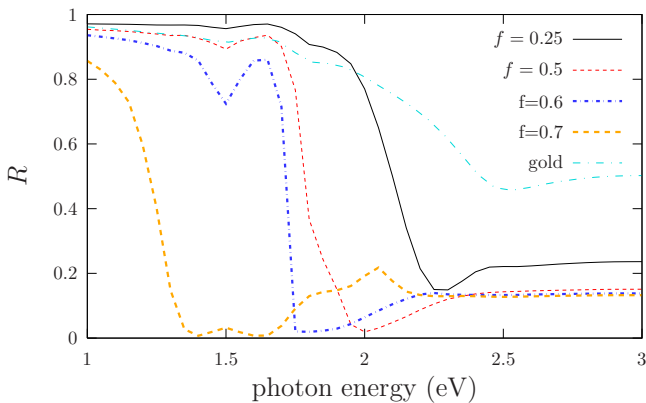


FIG. 8. (Color online) Reflectance $R_x=R_y=R$ vs photon energy for a system made up of circular cylinders with $\epsilon_p=4$ within an Au matrix $\epsilon_h=\epsilon(\text{Au})$ for four values of the filling fraction $f=0.25, 0.5, 0.6$, and 0.7 . We also show the reflectance of gold for comparison.

attains a minimum corresponding to the expected transition into a dielectric behavior. The transition frequency is red-shifted and becomes broader and deeper as f increases.

Our examples show that the reflection goes rapidly from almost one to almost zero at a frequency in the near infrared, which may be tuned by choosing the filling fraction and, in the case of rectangular inclusions, by changing the aspect ratio. A square array of cylinders is isotropic within the x - y plane, so, in a sense, the array of rectangular prisms is richer, as it allows us to change the behavior from conductinglike to insulatinglike by simply rotating the polarization.

We remark that the behavior of the reflection discussed above is induced solely by the geometry of the metamaterial and is not simply connected to the structure of the response functions of the constituent materials, that is, to resonances in ϵ_p and/or in ϵ_h . Similar resonances, mainly related to the geometry of the metamaterial, were already predicted by Khizhnyak¹⁶ back in 1958. Our results clearly show the huge difference that the shape of the inclusions makes on the optical properties of the system.^{11,12,38}

IV. CONCLUSIONS

We have developed a systematic scheme to calculate the complex frequency-dependent macroscopic dielectric function for metamaterials. Starting from Maxwell's equations and employing a long-wavelength approximation we have derived an expression for the macroscopic dielectric function ϵ_{ij}^M that depends on the dielectric functions of the host ϵ_h and particles ϵ_p , and on the geometry of both the unit cell and the inclusions. The calculation is set up through expansions of the microscopic fields in plane-wave components and in general a large number of reciprocal vectors \mathbf{G} are required to achieve convergence of the results. We validated our formalism through convergence tests and through comparison of our results to those from previous calculations finding an excellent agreement. Then, we calculated macroscopic response and the normal-incidence reflectivity for systems made up of dielectric rectangular prisms and cylinders arranged in a 2D square lattice within a gold host. Although the host and the inclusions are intrinsically isotropic, we found that if the inclusion is geometrically anisotropic so is the macroscopic optical response. For rectangular prisms of high aspect ratio we found a very anisotropic optical response, where the infrared reflectance is almost unity when the field is polarized along the long axis while it can attain values very close to zero when the field is polarized along the short axis. We explained this behavior in terms of a transition from a low-frequency conducting behavior to a high-frequency dielectric behavior for systems not too far from percolation into the nonconducting phase. The transition may occur at frequencies in the infrared frequencies for which one would naively expect very low values for the transmittance. We verified this explanation through the calculation of the reflectance of a square array of cylindrical prisms, which shows an isotropic but otherwise similar behavior as we approach the percolation threshold $f=\pi/4$. Our formalism may be employed to explore and design of very diverse systems with a tailored optical response. We hope this work would

motivate the construction of such systems and their optical characterization for the experimental verification of our results.

ACKNOWLEDGMENTS

We acknowledge inspiring discussions with Peter Halevi and Felipe Pérez-Rodríguez. This work was partially supported by DGAPA-UNAM under Grant No. IN120909 (W.L.M.), by CONACyT under Grant Nos. 48915-F (B.S.M.) and J49731-F (B.E.M.Z.), and by ANPCyT under Grant No. 190-PICTO-UNNE (G.P.O.).

APPENDIX

We show that our formalism, as embodied in Eqs. (11), (17), and (18), are equivalent in the nonretarded limit to the analytical results (27) and Eq. (28) for the case of periodically alternating isotropic thin flat slabs. We chose the y axis normal to the slabs so that the reciprocal vectors $\mathbf{G}=G\hat{y}$ lie all along y . In this case, both $[\mathcal{W}_0(G, G')]_{ij}$ and $[\epsilon_0(G, 0)]_{ij}$ are diagonal so we can consider separately the cases of polarization along the x and the y axes.

For x polarization we rewrite Eq. (11) as

$$\sum_{G' \neq 0} \left(\epsilon_h \delta_{GG'} + \epsilon_{ph} S(G - G') - \frac{G^2}{k_0^2} \delta_{GG'} \right) [\Phi_0(G', 0)]_{xx} = \epsilon_{ph} S(G), \quad (\text{A1})$$

whose solution is

$$[\Phi_0(G', 0)]_{xx} = 0 + \mathcal{O}(k_0^2/G^2). \quad (\text{A2})$$

Substitution in Eq. (17) yields immediately Eq. (27) to order 0 in the small quantities k_0/G in the nonretarded limit. Notice that the argument above is valid for any system that has translational invariance along one or more directions whenever the polarization direction points along those directions since Eq. (A1) holds when all the reciprocal vectors \mathbf{G} are perpendicular to the polarization direction. In particular, for systems that have texture only along two dimensions, the macroscopic dielectric function along the third dimension is simply the volume average of the microscopic dielectric functions.²⁵

For y polarization we rewrite Eq. (11) as

$$\sum_{G' \neq 0} [\epsilon_h \delta_{GG'} + \epsilon_{ph} S(G - G')] [\Phi_0(G', 0)]_{yy} = \epsilon_{ph} S(G), \quad (\text{A3})$$

where $G^2 - G_y G_y = 0$. Although $[\Phi_0(G, 0)]_{yy}$ is only defined for $G \neq 0$, we can extend its definition to $G=0$ by choosing $[\Phi_0(0, 0)]_{zz} \equiv 0$ and extending Eq. (A3) to include the $G=0$ term. For consistency, we have to add an unknown term to its RHS, which only applies to the $G=0$ term, i.e.,

$$\sum_{G'} [\epsilon_h \delta_{GG'} + \epsilon_{ph} S(G - G')] [\Phi_0(G', 0)]_{yy} = \epsilon_{ph} S(G) + C \delta_{G,0}, \quad (\text{A4})$$

where the sum includes now all values of G' . Taking the Fourier transform of Eq. (A4) we obtain

$$\epsilon_h [\Phi_0(y)]_{yy} + \epsilon_{ph} S(y) [\Phi_0(y)]_{yy} = \epsilon_{ph} S(y) + C, \quad (\text{A5})$$

which yields

$$[\Phi_0(y)]_{yy} = \frac{\epsilon_{ph} S(y) + C}{\epsilon(y)}. \quad (\text{A6})$$

The constant C must be chosen so that the spatial average of $[\Phi_0(y)]_{yy}$ vanishes,

$$0 = [\Phi_0(G=0, 0)]_{yy} = \frac{1-f}{\epsilon_h} C + \frac{f}{\epsilon_p} (\epsilon_{ph} + C). \quad (\text{A7})$$

Substituting the result in Eq. (A6) we obtain

$$[\Phi_0(y)]_{yy} = \frac{\epsilon_{ph}}{\epsilon(y)} \left[S(y) - \frac{f \epsilon_h}{\epsilon_h + \epsilon_{ph}(1-f)} \right]. \quad (\text{A8})$$

Now we extend the sum in Eq. (17) to include the $G=0$ contribution allowing us to employ the convolution theorem to obtain

$$\begin{aligned} \sum_G S(-G) [\Phi_0(G, 0)]_{yy} &= \frac{1}{L_y} \int dy S(y) [\Phi_0(y)]_{yy} \\ &= f \frac{\epsilon_{ph}}{\epsilon_p} \left(1 - \frac{f \epsilon_h}{\epsilon_h + \epsilon_{ph}(1-f)} \right), \end{aligned} \quad (\text{A9})$$

which we substitute into Eq. (17) to finally obtain Eq. (29).

¹ *Electrical Transport and Optical Properties of Inhomogeneous Media*, edited by J. C. Garland and D. B. Tanner, AIP Conf. Proc. No. 40 (American Institute of Physics, New York, 1978).

² *Electrical Transport and Optical Properties of Inhomogeneous Media*, edited by W. Mochán and R. G. Barrera (Elsevier, The Netherlands, 1994).

³ *Electrical Transport and Optical Properties of Inhomogeneous Media*, edited by G. Milton, K. Golden, D. Dobson, and A. Vardeny (Elsevier, North-Holland, 2003).

⁴ Z. Hashin and S. Shtrikman, *J. Appl. Phys.* **33**, 3125 (1962).

⁵ W. L. Mochán and R. G. Barrera, *Phys. Rev. B* **32**, 4984 (1985).

⁶ J. B. Keller, *J. Appl. Phys.* **34**, 991 (1963).

⁷ J. B. Keller, *J. Math. Phys.* **5**, 548 (1964).

⁸ J. Nevard and J. B. Keller, *J. Math. Phys.* **26**, 2761 (1985).

⁹ Y. Akahane, T. Asano, B.-S. Song, and S. Noda, *Nature (London)* **425**, 944 (2003).

¹⁰ A. N. Grigorenko, A. K. Geim, H. F. Gleeson, Y. Zhang, A. A. Firsov, I. Y. Khrushchev, and J. Petrovic, *Nature (London)* **438**,

- 335 (2005).
- ¹¹K. J. Klein Koerkamp, S. Enoch, F. B. Segerink, N. F. van Hulst, and L. Kuipers, *Phys. Rev. Lett.* **92**, 183901 (2004).
- ¹²R. Gordon, A. G. Brolo, A. McKinnon, A. Rajora, B. Leathem, and K. L. Kavanagh, *Phys. Rev. Lett.* **92**, 037401 (2004).
- ¹³J. B. Pendry, *Phys. Rev. Lett.* **85**, 3966 (2000).
- ¹⁴V. M. Shalaev, W. Cai, U. Chettiar, H. Yuan, A. Sarychev, V. Drachev, and A. Kildishev, *Opt. Lett.* **30**, 3356 (2005).
- ¹⁵A. Kildishev, W. Cai, U. Chettiar, H.-K. Yuan, A. Sarychev, V. P. Drachev, and V. M. Shalaev, *J. Opt. Soc. Am. B* **23**, 423 (2006).
- ¹⁶N. Khizhnyak, *Sov. Phys. Tech. Phys.* **4**, 539 (1959).
- ¹⁷R. C. McPhedran and D. R. McKenzie, in *Electrical Transport and Optical Properties of Inhomogeneous Media*, edited by J. C. Garland and D. B. Tanner, AIP Conf. Proc. No. 40 (American Institute of Physics, New York, 1977), p. 294.
- ¹⁸W. T. Doyle, in *Electrical Transport and Optical Properties of Inhomogeneous Media*, edited by J. C. Garland and D. B. Tanner, AIP Conf. Proc. No. 40 (American Institute of Physics, New York, 1977), p. 300.
- ¹⁹F. Claro, *Phys. Rev. B* **30**, 4989 (1984).
- ²⁰R. Rojas and F. Claro, *Phys. Rev. B* **34**, 3730 (1986).
- ²¹W. L. Mochán and R. G. Barrera, *Phys. Rev. B* **32**, 4989 (1985).
- ²²L. Li, *J. Opt. Soc. Am. A Opt. Image Sci. Vis* **14**, 2758 (1997).
- ²³R. Tao, Z. Chen, and P. Sheng, *Phys. Rev. B* **41**, 2417 (1990).
- ²⁴L. Shen, C. Liu, J. Korryng, and K. Dunn, *J. Appl. Phys.* **67**, 7071 (1990).
- ²⁵A. A. Krokhin, P. Halevi, and J. Arriaga, *Phys. Rev. B* **65**, 115208 (2002).
- ²⁶P. Halevi, A. A. Krokhin, and J. Arriaga, *Phys. Rev. Lett.* **82**, 719 (1999).
- ²⁷S. Datta, C. T. Chan, K. M. Ho, and C. M. Soukoulis, *Phys. Rev. B* **48**, 14936 (1993).
- ²⁸R. Fuchs, in *Electrical Transport and Optical Properties of Inhomogeneous Media*, edited by J. C. Garland and D. B. Tanner, AIP Conf. Proc. No. 40 (American Institute of Physics, New York, 1977), p. 276.
- ²⁹G. Milton, *J. Appl. Phys.* **52**, 5294 (1981).
- ³⁰D. J. Bergman and K. J. Dunn, *Phys. Rev. B* **45**, 13262 (1992).
- ³¹P. Sheng, R. S. Stepleman, and P. N. Sanda, *Phys. Rev. B* **26**, 2907 (1982).
- ³²H. Lochbihler and R. Depine, *Appl. Opt.* **32**, 3459 (1993).
- ³³H. Lochbihler, *Phys. Rev. B* **50**, 4795 (1994).
- ³⁴H. F. Ghaemi, T. Thio, D. E. Grupp, T. W. Ebbesen, and H. J. Lezec, *Phys. Rev. B* **58**, 6779 (1998).
- ³⁵S. A. Darmanyan and A. V. Zayats, *Phys. Rev. B* **67**, 035424 (2003).
- ³⁶J. A. Porto, F. J. García-Vidal, and J. B. Pendry, *Phys. Rev. Lett.* **83**, 2845 (1999).
- ³⁷D. C. Skigin and R. A. Depine, *Phys. Rev. Lett.* **95**, 217402 (2005).
- ³⁸F. J. García-Vidal, E. Moreno, J. A. Porto, and L. Martín-Moreno, *Phys. Rev. Lett.* **95**, 103901 (2005).
- ³⁹P. Halevi and F. Pérez-Rodríguez, in *Proceedings of Society of Photo-Optical Instrumentation Engineers (SPIE) Conference Series* (2006), Vol. 6320, p. 63200T-1–9.
- ⁴⁰G. Milton, R. McPhedran, and D. MCKenzie, *Appl. Phys.* **25**, 23 (1981).
- ⁴¹H. S. Sozuer, J. W. Haus, and R. Inguva, *Phys. Rev. B* **45**, 13962 (1992).
- ⁴²A. A. Krokhin, E. Reyes, and L. Gumen, *Phys. Rev. B* **75**, 045131 (2007).
- ⁴³*Handbook of Optical Constants of Solids*, Academic Press Handbook Series, edited by E. D. Palik (Academic, Orlando, FL, 1985).
- ⁴⁴The numerical burden of such large matrices has to be surmounted with the use of ScaLAPACK subroutines (<http://www.netlib.org/scalapack/>) to efficiently solve Eq. (11) on a high-end computer cluster. Typical time on 40-processor grid is 1.3 h per energy point.